EI SEVIER

Contents lists available at ScienceDirect

Remote Sensing of Environment

journal homepage: www.elsevier.com/locate/rse



Effect of spatial variability of wet snow on modeled and observed microwave emissions



Carrie M. Vuyovich ^{a,*}, Jennifer M. Jacobs ^b, Christopher A. Hiemstra ^a, Elias J. Deeb ^a

- ^a Cold Regions Research and Engineering Laboratory, 72 Lyme Road, Hanover, NH 03755, United States
- ^b University of New Hampshire, 240 Gregg Hall, 34 Colovos Road, Durham, NH 03824, United States

ARTICLE INFO

Article history:
Received 31 October 2016
Received in revised form 3 May 2017
Accepted 8 June 2017
Available online xxxx

Keywords:
Brightness temperature
Liquid water content
Snow
Passive microwave
Emission model
MEMLS
Wet snow
AMSR-E

ABSTRACT

Melting snow provides an essential source of water in many regions of the world and can also contribute to devastating, wide-scale flooding. Global datasets of recorded passive microwave emissions provide non-destructive, daily information on snow processes including the presence of liquid water in the snow, which can be an indicator of snowmelt. The objective of this research is to test the sensitivity of the emission signal as it relates to the spatial distribution of liquid water content in the snowpack. This signal response was evaluated over an area approximately the size of a microwave pixel to assess whether a relationship exists between the aerial extent of wet snow and the magnitude of the T_R response. A sensitivity analysis was performed using a high-resolution, physically based snow-emission model to simulate microwave emissions. The signal response to wet snow was evaluated given a range of spatially distributed snowpack conditions. Daily snow states were simulated for a 9-year period using a high-resolution (50 m) energy balance snow model over a 34×34 km domain. These data were fed into a microwave emission model to simulate brightness temperatures. A near-linear relationship was found between the T_B signal response over a spatially heterogeneous snowpack and the percent area with liquid water content (LWC) present. The results were confirmed by evaluating actual wet snow events over a 9-year period. The model output was also compared to AMSR-E passive microwave satellite data and discharge data at a basin outlet within the study area. The results are used to help understand the impact of spatially distributed snowmelt as detected by passive microwave data.

Published by Elsevier Inc.

1. Introduction

In snow-dominated basins, efficient water resource management requires accurate, timely estimates of both snow water equivalent (SWE) and snow melt onset. Melting snow provides a reliable water supply and can also produce wide-scale flooding, particularly when combined with rainfall. For hydrological purposes, an accurate estimate of the melt distribution is essential for correctly predicting the runoff response (Lundquist and Dettinger, 2005), and will also provide insight into important ecological and biogeochemical processes (Bales et al., 2006). However, snow characteristics can be highly variable across a land-scape, and techniques for accurately characterizing the spatial distribution of snow properties remains elusive (Elder et al., 1998; Dozier et al., 2016).

The presence of liquid water in an existing snowpack, which can be an indicator of snowmelt, is particularly difficult to measure or detect over large areas (Kang et al., 2014). Increasingly over the past 30 years, satellite remote sensing techniques have been investigated for mapping wet snow (Tedesco, 2015). Optical and infrared imagery

* Corresponding author.

E-mail address: carrie.m.vuyovich@usace.army.mil (C.M. Vuyovich).

have been used to estimate snow melt based on albedo and surface temperature observations (Green et al., 2002). These data have the benefit of high spatial and temporal resolution, but are unable to observe the snow cover through cloud cover or at night. Microwave measurements are highly sensitive to the snowpack electromagnetic properties as the snow transitions from dry to wet (Mätzler et al., 1980). These data are minimally impacted by atmospheric conditions and do not require daylight to make observations. Synthetic Aperature Radar (SAR) C-band and X-band instruments have been used to accurately resolve wet snow on a hillslope scale at a high resolution (Nagler and Rott, 2000). However, because of the small swath size, SAR data are currently not suitable for monitoring snow melt over large regions. For basin-scale observations, passive and active microwave sensors have been used to estimate the timing of melt onset and detect wet snow. Active microwave sensors measure a reduced backscatter signal when liquid water is present in snow, caused by a significant change in the imaginary part of the snow effective permittivity. Scatterometer sensors have been used to map areas of active snow melt and the data have been shown to correlate to basin discharge events (Nghiem and Tsai, 2001; Rawlins et al., 2005).

Passive microwave observations are also sensitive to the presence of liquid water in the snow and have the benefit of a long historical record

(since 1979). Microwave emissions are measured in units of brightness temperature (T_B), which in the microwave spectrum is equal to the thermometric temperature of the emitting material times the emissivity. Satellite measurements of T_B include primarily emissions from the Earth as well as reflected radiation from the sky. Ground emission signals can be affected as they pass through snow, vegetation and the atmosphere. The presence of snow causes signal scattering at certain frequencies. As a result, the measured T_B decreases due to signal extinction through the snowpack. Empirical SWE formulations relate snow depth to the difference between two microwave frequencies: one that scatters as it passes through snow and one that does not, approximately 36 and 18 GHz, respectively (Chang et al., 1982).

Microwave emissions are highly responsive to liquid water content (LWC), the volume of liquid water per unit volume of snow, due to the sensitivity of the radiance to changes in the dielectric constant (Stiles and Ulaby, 1980). The presence of water within a snowpack increases the emissivity resulting in a sharp T_B increase (Davis et al., 1987; Mätzler, 1987; Walker and Goodison, 1993). Passive microwave emissions cannot be used to estimate SWE during wet snow periods because of the reduced signal scattering. However, the signal response provides a clear indication of increased liquid water content, which overwhelms the impact of other snowpack properties on the microwave signal (Wang et al., 2001). T_B increases occur with as little as 1-2% liquid water content in the snowpack (Cagnati et al., 2004; Stiles and Ulaby, 1980; Tedesco et al., 2006). While 1% LWC is not enough to cause runoff, the satellite response to a wide-spread wet snow event likely indicates a significant melting or rain-on-snow event and greater than 1% LWC. Several studies have linked the microwave response at a coarse resolution to basin runoff and shown potential for hydrologic applications (Ramage and Semmens, 2012; Vuyovich and Jacobs, 2011; Yan et al., 2009).

For over three decades, studies have investigated using this response to predict melt onset (Kunzi et al., 1982; Drobot and Anderson, 2001; Ramage et al., 2006), or to identify rain-on-snow (ROS) events (Grenfell and Putkonen, 2008). Two approaches have been developed to detect the timing of snowmelt using microwave signal response to wet snow. The Diurnal Amplitude Variation (DAV) approach identifies the onset of melt using the large differences in T_B between the morning and afternoon overpasses at the 37 GHz frequency (Kopczynski et al., 2008; Ramage et al., 2006; Tedesco et al., 2009). A DAV increase indicates the onset of the daytime melt/night-time refreeze cycle and the beginning of spring snowmelt. The high-DAV period that follows the onset of melt, referred to as the transition period, ends when the snowpack is continuously melting during day and night periods and the brightness temperature difference decreases. Another method uses the gradient and polarization ratios (GR and PR, respectively) to isolate the bulk emissivity of the snowpack and identify significant rain-onsnow events. In the Canadian Arctic, Grenfell and Putkonen (2008) demonstrated that the GR and PR can be used to identify the occurrence as well as the intensity of rain-on-snow events. Using a combination of these two approaches, Semmens et al. (2013) developed an algorithm for detecting early season melt events with AMSR-E passive microwave data, and were able to successfully identify melt events caused by both rain-on-snow and snowmelt alone.

These methods have successfully demonstrated an ability to detect the timing of snowmelt, which has implications for runoff; however, they do not provide information on the volume of runoff. The discharge magnitude during a snowmelt event is a function of the snowpack properties as well as the spatial extent over which snowmelt is occurring. An improved understanding of the satellite retrievals' response to the spatially distributed snowmelt is needed. Kang et al. (2014) and Pan et al. (2014) conducted the foundation work needed to characterize footprint scale emissions. They used the Microwave Emission Model for Layered Snowpacks (MEMLS) and the Helsinki University of Technology (HUT) snow microwave radiative transfer models, respectively, to successfully capture the emission signatures in wet snowpacks and compare the

results to point observations. Both studies report a sharp increase in the T_B response immediately after wetting (the signal response used in detecting the onset of melt) despite differences in snowpack characteristics and wetness profiles.

The goal of this study is to understand the T_B response to spatially distributed wet snow within a satellite pixel and to begin to evaluate the relationship between the aggregated T_B response and river discharge. In this study, we investigate the sensitivity of T_B to spatially distributed wet snow using loosely coupled, physically-based snow and emission models. A long-term ecological research area in the northeast U.S. was selected as the study location because of its long record of meteorological, hydrological and snow observations (described in Section 2). The methods used to develop a relationship between the change in T_B and the fractional area affected by wet snow are described in Section 3. These include a sensitivity analysis to assess the impacts of artificially distributed LWC on the emission signal, and evaluation of the simulated and observed T_B during wet snow events over a nine year period. Results of the analysis are provided in Section 4 and include a comparison of the T_R response and increases in observed streamflow during wet snow events. In Section 5 we discuss the implications of these results with potential future directions.

2. Study area and data

The study domain is a 34 km by 34 km area in the White Mountains of New Hampshire, USA which includes the Hubbard Brook Experimental Forest (HBEF), a Long Term Ecological Research (LTER) watershed (Fig. 1). The HBEF watershed has an area of 31.6 km², which covers approximately 3% of the total study domain and is representative of the larger area. HBEF has more than 50 years of meteorological and hydrological observations, which have enabled decades of ecologic and hydrologic research. Approximately one-third of the annual precipitation falls as snow, with a mean annual maximum SWE for the period of record at HBEF of approximately 189 mm, and a snow cover that generally persists from mid-December to mid-April (Campbell et al., 2007).

The study domain is a mountainous region, characteristic of the northeastern United States Appalachian Mountains with elevations ranging from 120 to 1470 m. Land cover is Eastern Deciduous Forest, with evergreen forest and tundra at the highest elevations. Agricultural and developed areas are primarily limited to the lowest elevations and along rivers. Elevation data for the domain were developed from 30 m resolution National Elevation Data (NED) (USGS, 2009). Land cover data were obtained from the National Land Cover Database (NLCD) (Homer et al., 2015). Both the elevation and land cover data were clipped and resampled to a 50 m resolution. Stream channels in this region are generally steep with coarse-grained bed material. A shallow soil layer, with underlying bedrock approximately 1–2 m below the surface, means minimal loss to deep groundwater and relatively quick runoff response (Campbell et al., 2011). Discharge records demonstrate a seasonal snowmelt signal with the highest runoff volumes occurring in March-May.

Meteorological and snow course data from 1 October 2002 to 30 September 2011 at the Hubbard Brook LTER (Bailey et al., 2003) and National Weather Service stations were used in this study (Table 1). Daily temperature and precipitation observations were available from approximately 10 locations each year. The Hubbard Brook LTER data provided precipitation measurements over a representative elevation range. Relative humidity, wind speed and direction were available at three of the 10 observation stations. Only two stations lacked complete data coverage for the entire period of interest. Snow water equivalent was measured at five Hubbard Brook snow course locations on a weekly basis. HBEF also maintains an NRCS Soil Climate Analysis Network (SCAN) site; an automated station with a snow pillow to measure SWE, as well as measurements of snow depth, soil moisture and numerous meteorological variables. The station has been collecting hourly data since 2002.

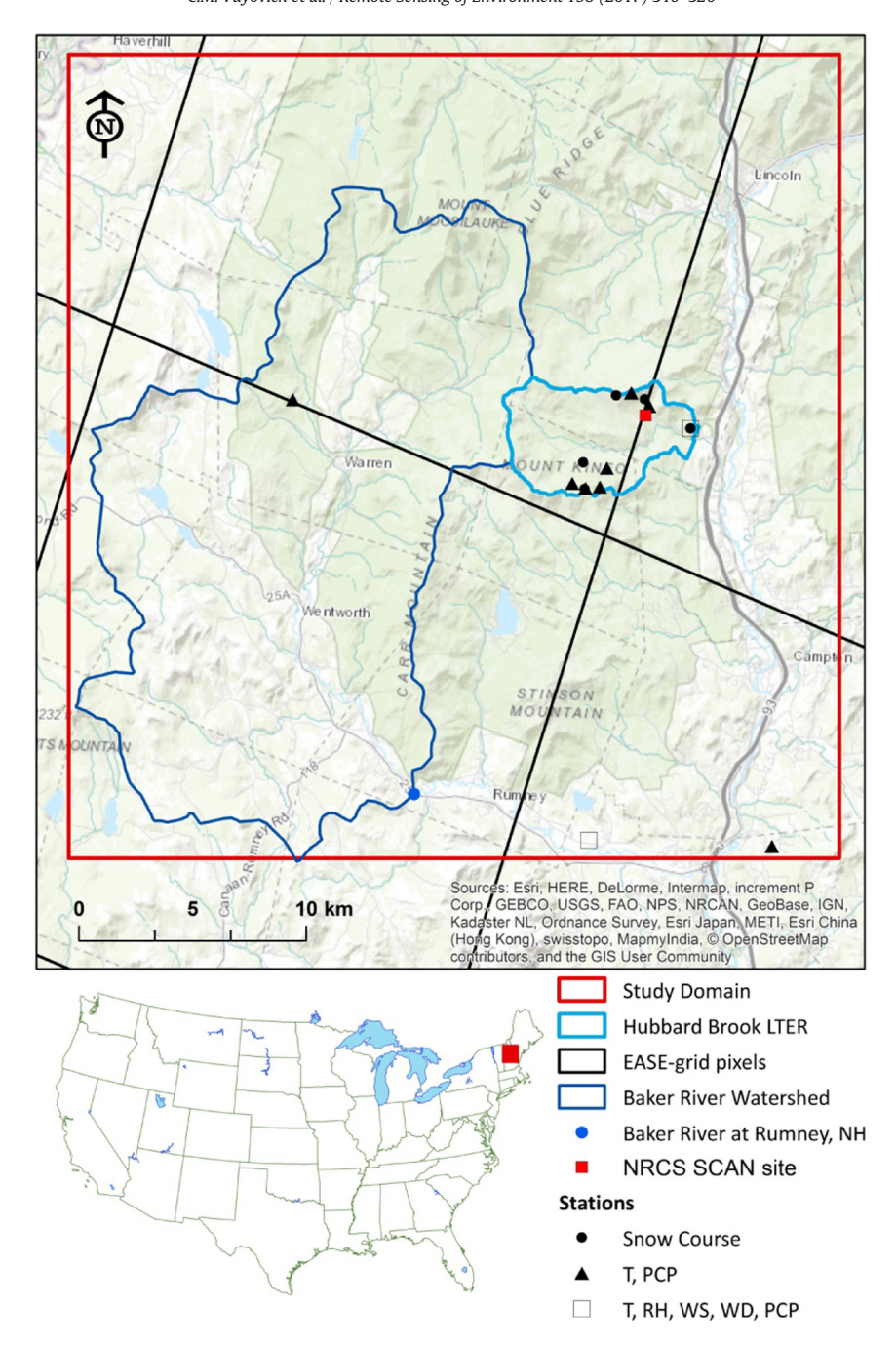


Fig. 1. Study region, located in the White Mountains of New Hampshire, US.

Within the HBEF research area, nine instrumented watersheds have recorded continuous discharge measurements since 1956 (Bailey et al., 2003). Additionally, the Baker River watershed is an unregulated basin, with an area of approximately 370 km², which is entirely contained within the study domain but outside of HBEF. Streamflow data were obtained for the Baker River at Rumney, NH from the U.S. Geological Survey (USGS, 2001).

Passive microwave brightness temperature data from the Advanced Microwave Scanning Radiometer-Earth Observing System (AMSR-E) were obtained from the National Snow and Ice Data Center (NSIDC) (Cavalieri et al., 2014). AMSR-E was launched on NASA's Aqua satellite in 2002 and data are available through 2011 in Equal-Area Scalable Earth (EASE)-grid projection as 25-km grids. Horizontally and vertically

polarized T_B measured at frequencies 18.7 and 36.5 GHz were used in this analysis to match the frequencies primarily used in empirical formulations to estimate snow mass. AMSR-E data are available twice daily: ascending passes that occur in the afternoon and descending passes that occur in the early morning. This study used the descending passes only to focus on wide-spread, continuous melt events rather than diurnal melt signals that do not contribute as much to discharge. The analysis was only looked at melt events prior to when snowmelt was actively occurring over the entire domain, though some earlier melt events may have resulted in melt-refreeze cycles which can cause increased scattering and low T_B estimates (Clifford, 2010). For each descending overpass during the nine-year period of record, an area-weighted average T_B was computed over the study domain, at

Table 1List of meteorological stations and snow survey sites used.

Station name (ID)	Lat.	Long.	Elev. (m)	Observations ^a	Water years used
Hubbard Brook HQ (STA HQ)	43.94	-71.70	255	T, RH, WS, WD, PCP, SWE	2003-2011
Hubbard Brook 1A (STA 1A)	43.95	-71.73	490	T, PCP	2003-2011
Hubbard Brook Station 2 (STA 2)	43.95	-71.73	561	SWE	2003-2011
Hubbard Brook Station 6 (STA 6)	43.96	-71.74	740	T, PCP	2003-2011
Hubbard Brook Station 9 (STA 9)	43.96	-71.74	762	SWE	2003-2011
Hubbard Brook Station 14 (STA 14)	43.92	-71.77	740	T, PCP	2003-2011
Hubbard Brook Station 17 (STA 17)	43.92	-71.76	740	T, PCP, SWE	2003-2011
Hubbard Brook Station 19 (STA 19)	43.92	-71.76	792	SWE	2003-2011
Hubbard Brook Station 23 (STA 23)	43.93	-71.76	669	T, PCP	2003-2011
Hubbard Brook Station 24 (STA 24)	43.92	-71.75	796	T, PCP	2003-2011
NRCS SCAN Site	43.93	-71.72	460	T, PCP, WS, WD, RH, SWE	2003-2011
Plymouth Mun. Airport	43.78	-71.75	157	T, RH, WS, WD, PCP	2006-2011
Plymouth COOP Station	43.78	-71.65	303	T, PCP	2003-2008
Wentworth COOP Station	43.95	-71.92	282	PCP	2003-2011
Mt. Wash Regl. Airprt.b	44.37	-71.54	327	T, RH, WS, WD, PCP	2003-2011

 $[\]label{eq:continuous} \begin{subarray}{l} a \\ T = temperature (\begin{subarray}{l} \begin{subarray}{l} \$

both frequencies and polarizations, as:

$$T_{B(f,P),j} = \sum_{i=1}^{n} T_{B,i,j} A_{i}$$
 (1)

where $T_{B(f,P),j}$ is the area-weighted average T_B at frequency, f, and polarization, *P*, over the domain for overpass, *j*; *n* is the number of pixels with some portion in the domain; $T_{B,i,j}$ is the T_B for pixel, i, during overpass, j; and A_i is the fractional area of pixel, i, located within the domain. A gap in the satellite swath coverage over the region of interest occurs every 3 to 4 days. Values were only computed for images when no data were missing within the study domain. Earlier work by Vuyovich et al. (2014) found that vegetation in this region of the U.S. impacts of accuracy of empirically-based passive microwave SWE estimates, causing an underestimation of SWE and introducing scatter to the signal. This agrees with numerous other studies evaluating the effects of vegetation on passive microwave SWE estimates (Derksen et al., 2003; Foster et al., 2005). In this study no corrections were made to the satellite observations to adjust for vegetation. The satellite T_B was compared to model results to evaluate the signal response to wet snow even with vegetation impacts.

3. Methods

For this analysis, a physically-based snow model was loosely coupled with a microwave emission model to simulate the snowpack radiance over a 9-year period, 2003–2011. Loosely coupled refers to modules run independently to each other with minimal interdependence. In this context, results from the snow model were fed into the microwave emission model with no knowledge or dependence of the underlying processes. A single layer snow model was used to focus the analysis on the impacts of LWC. The models were run at a 50 m resolution over the study domain with a daily time step. Fig. 2 provides a diagram of the process.

3.1. Snow and microwave emission models

SnowModel was used to simulate the snow evolution in the study domain and estimate spatially distributed snow characteristics including snow depth, temperature and, density, SWE, albedo and snowmelt. SnowModel combines an energy balance snow model, and a wind redistribution model to simulate spatially distributed snow cover evolution under a variety of landscapes and conditions (Liston and Elder, 2006a). MicroMet, a high-resolution atmospheric model (Liston and Elder, 2006b) was used to distribute and downscale the required meteorological forcing data. SnowAssim (Liston and Hiemstra, 2008) was used to assimilate SWE field observations. SnowAssim uses an optimal interpolation approach (Gandin, 1965) developed from differences between an initial condition simulation SWE and observed coincident SWE to yield spatially-distributed precipitation correction fields used for a subsequent simulation (Liston and Hiemstra, 2008). The HBEF snow course data were assimilated into the model at approximately bi-weekly intervals over the simulation period to better match the snow observations. SWE measurements from the SCAN site, which were not assimilated, were then used to validate model results.

The Microwave Emission Model of Multilayered Snowpack (MEMLS) was used to estimate the microwave emissions over the study domain, with snow characteristics provided from SnowModel output. MEMLS is a semi-empirical radiative transfer model that simulates the scattering effect of snow on microwave emissions at frequencies ranging from 5 to 100 GHz using multiple scattering radiative theory (Mätzler and Wiesmann, 1999; Wiesmann and Mätzler, 1999). MEMLS estimates internal scattering based on six-flux theory, which is simplified for upwelling and downwelling radiation. Scattering coefficients are determined based on characteristics of the snow.

MEMLS was used to estimate vertically and horizontally polarized T_B through the snow at 18.7 and 36.5 GHz to match the AMSR-E frequencies used to estimate SWE. The 36.5 GHz frequency is of particular interest and the focus of this paper because of its sensitivity to snow

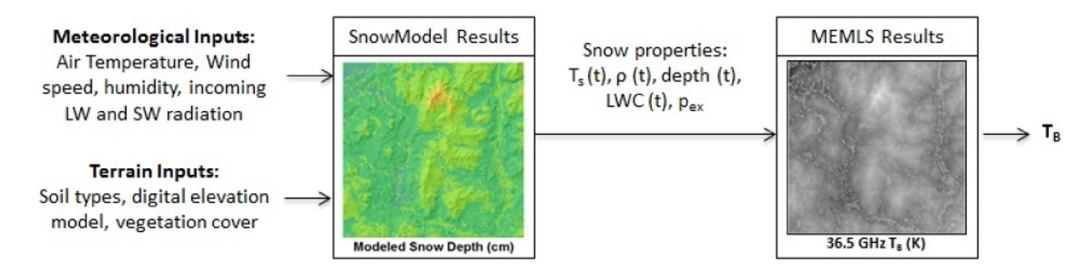


Fig. 2. Diagram of the coupled modeling process over the 34 km \times 34 km domain.

^b Located outside of the domain.

parameters (Tedesco and Kim, 2006). Snow characteristics including snow depth, density, temperature, liquid water content (LWC), and the exponential correlation length ($p_{\rm ex}$) are required as input to MEMLS. Snow temperature, depth and density were used directly from SnowModel output. The $p_{\rm ex}$ is a metric for grain size used in MEMLS to estimate the scattering coefficient. The original approach assumed $p_{\rm ex}$ values ranging from 0.05–0.3 mm (Wiesmann and Mätzler, 1999), which was later extended to handle coarse grains up to 0.6 mm (Mätzler and Wiesmann, 1999). SnowModel does not simulate grain size. To focus the investigation on the effects of LWC, a constant $p_{\rm ex}$ was used for all grid cells.

3.2. Sensitivity analysis

The first sensitivity analysis was conducted to develop a relationship between the T_B response and the percent LWC in the snow, uniformly distributed across the study domain. A single date was selected when the study domain was 100% snow covered and no LWC was present in the snow based on SnowModel results. This provided a realistic spatial distribution of snow characteristics with which to test the effects of LWC. In the first series of simulations, LWC was applied across the domain as a constant percentage of the SWE in each grid cell. The LWC was uniformly applied to each grid cell in 0.1% increments increasing from 0 to 5%. In the next series of simulations, the same adjustment to LWC performed in the first test was repeated while individually adjusting the other snow characteristics. The snow depth, density, temperature and exponential correlation length were varied between a selected maximum and minimum average value over the study domain. To adjust the snow depth, density and temperature, the individual grid cell values were scaled by the ratio of the new domain average value to the original average. The exponential correlation length was uniformly adjusted across the domain to represent a range of expected grain sizes from fine to coarse.

In the second sensitivity analysis, LWC was applied to increasing areas of the study domain using SnowModel results on the same date as in the previous analysis. The area assigned LWC was increased from 0% to 100% by 10% increments. The goal of this analysis was to develop a relationship between the percent area impacted by wet snow and the change in T_B over the entire domain. Two different spatial distributions were used to assign LWC to the grid cells: random and by elevation. The random distribution assigned LWC to grid cells at random. The elevation distribution assigned LWC to grid cells beginning with the lowest elevations first, and increasing the percent area within the domain as a function of elevation. The elevation distribution was used to replicate a more realistic melt pattern, which is often strongly correlated with elevation, though it is not the only factor (Lundquist et al., 2004). Table 2 provides a matrix of the tests performed in the sensitivity analysis.

3.3. Wet snow events

For the period 2003–2011, the snow emission model was run over each winter season and wet snow events were identified using a

threshold change in T_B greater than 5 K from the previous day. The threshold was used to filter out small increases in T_B that could be due to minor melt events, and was selected as a value greater than one standard deviation of the one-day change in TB over the nine winter seasons. To ensure that the domain was mostly snow covered, the events were limited to the December to March time period when the average SWE over the domain was at least 10 mm. SnowModel output includes snowmelt but not LWC, a snow property required by MEMLS. In grid cells where SnowModel estimated snow melt runoff greater than zero, LWC was assumed to be present in the snowpack. For each event identified, the change in the observed T_B was compared with the results of the sensitivity analysis. For significant melt events to occur the snowpack temperature must be at the melt temperature, 273.15 K. For each wet snow event, the change in brightness temperature from one day, $T_{B,1}$, to the next, $T_{B,2}$, was normalized by the difference between the previous day's T_B and 273.15 K, which represents the largest change in T_B that could occur. The normalized brightness temperature, $T_{B,n}$ is defined

$$T_{B,n} = \frac{(T_{B,2} - T_{B,1})}{(273.15 \, K - T_{B,1})} \tag{2}$$

The AMSR-E 36.5 GHz T_B was compared to the modeled T_B over the period, 2003–2011 when the satellite data are available. The normalized change in AMSR-E T_B during the wet snow events was also compared to the results of the sensitivity analysis.

For each wet snow event identified, discharge changes in the Baker River at Rumney, NH were quantified. While not all wet snow packs will result in runoff, liquid water detected in the snowpack is a necessary precursor to winter discharge increase. The absolute change in discharge for up to 4 days following a wet snow event identified in the microwave signal was compared to the change in T_B estimated from MEMLS and AMSR-E. Four days was selected based on a review of historical discharge records at the Baker River station to allow sufficient time for the snow melt runoff to drain from the basin and reach a peak discharge, but not so much that the hydrograph included multiple events or had begun to recede.

4. Results

4.1. High-resolution simulation of snow characteristics over study domain

SnowModel results were validated using observed SWE at an NRCS SCAN site located within the Hubbard Brook watershed which was not assimilated into the model. Over the 9 years when both snow pillow observations and SnowModel results were available, the correlation (R^2) between the daily SWE data was 0.82 indicating a close match between the modeled and observed at that location. The study area is usually completely snow covered during the winter months, beginning on 10 December and ending on 8 May on average. The average peak SWE date occurs on 10 March, and the estimated average peak SWE over the study domain during the 9-year time period is 172 mm. The

Table 2Sensitivity analysis test matrix, using SnowModel results on 11 March 2003.

LWC analysis	Snow depth ^a (cm)	Snow temp. ^a (K)	Snow density ^a (kg/m ³)	Exponential correlation length, pex
Tests 1–5: Uniform application of vary	ing LWC across domain, 51 sim	ulations increasing LWC from 0-5	% by 0.1% increments	
Test 1: baseline	49 cm	266.8 K	301.7 kg/m ³	0.11
Test 2: adjusting snow depth	2 Tests: 25 cm and 80 cm	266.8 K	301.7 kg/m ³	0.11
Test 3: adjusting snow temperature	49 cm	3 Tests: 250, 260 and 270 K	301.7 kg/m ³	0.11
Test 4: adjusting snow density	49 cm	266.8 K	2 Tests: 200 and 400 kg/m ³	0.11
Test 5: adjusting p _{ex}	49 cm	266.8 K	301.7 kg/m ³	2 Tests: $p_{\rm ex} = 0.3$ and 0.65
Tests 6–7: Spatial distribution of consta	ant LWC across domain, 11 sim	ulations, LWC = 1% , assigned to 0	-100% of the area by 10% increme	ents
Test 6: LWC assigned randomly	49 cm	266.8 K	301.7 kg/m ³	0.11
Test 7: LWC assigned by elevation	49 cm	266.8 K	301.7 kg/m ³	0.11

^a Average over domain.

maximum peak SWE was 311 mm in 2008 and a minimum peak SWE of 78 mm was estimated in 2006. Simulated snow depths showed variability with topography, which agrees with observed snow measurements. SWE measured at HBEF are consistently deeper at high-elevations than in the valley floors throughout the snow accumulation and ablation season. In addition, melt rates, calculated as the average positive decrease in snow depth on each day of the year, are greater at the lower elevations earlier in the season and at the higher elevations later in the season (Fig. 3). This supports the use of elevation as a realistic index for snowmelt patterns.

4.2. Simulation of snow microwave emissions over study domain

The MEMLS model was run for each 50×50 m grid cell over the 9 year study period, using snow characteristics from SnowModel as input. The results were averaged to provide a single T_B for the whole study domain, which were then compared to the vertically polarized 36.5 GHz T_B from the AMSR-E satellite sensor. Though no atmospheric or vegetation corrections were made to the AMSR-E data for this study, both measured and modeled T_B show a similar decrease during the winter months when snow is impacting the signal (Fig. 4). The R² and RMSE between the modeled and observed data are 0.53 and 8.3 K, respectively. T_B estimates range from approximately 273 K during the snow-free periods to 220–240 K at the peak snowpack. In 2005 and 2006 there are larger differences between the data than other years. Both years experienced a shallow snowpack compared to other years, particularly in the beginning of the season, which may have impacted the satellite results. Dissimilarities between the data could also be due to atmospheric or vegetation effects on the AMSR-E data or model assumptions.

4.3. Sensitivity of microwave emissions to LWC in snow

The sensitivity analysis provided the foundation to examine the effect of LWC on microwave emissions over the study domain. On the date selected for the sensitivity analysis, 11 March 2003, SnowModel results estimated 100% snow cover over the domain and no LWC (Fig. 5). The average snow depth on this date was 49.1 cm, ranging from a maximum of 145.2 cm to a minimum of 13.7 cm across the study domain. The average snow density and temperature were 301.7 kg/m³ and -6.32 °C (266.8 K), respectively. A constant p_{ex} of 0.11 was used for all grid cells based on observed values for a similar snowpack depth (Proksch et al., 2015; Wiesmann et al., 1998). The 36.5 GHz T_B, estimated by MEMLS on this date, was 248.6 and 237.6 K for the vertical and horizontal polarizations, respectively. The computed 18.7 GHz T_B on this date was 266.1 K for the vertical polarization and 253.3 K for the horizontal polarizations. For comparison, the AMSR-E T_B observed on this date were 229.7 and 226.4 K for the vertical and horizontal polarizations of the 36.5 GHz frequency, respectively. The T_B observations

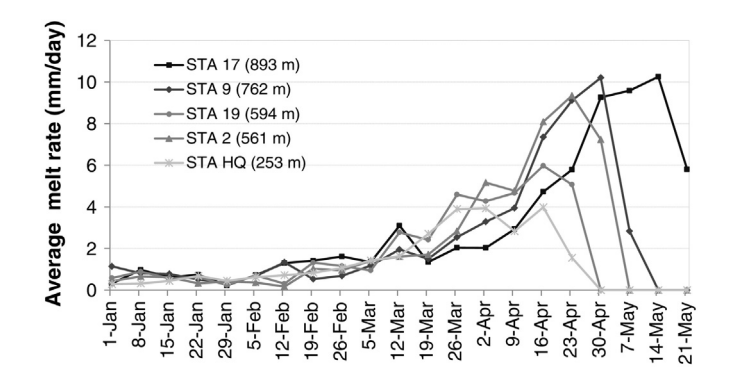


Fig. 3. Average daily melt rates at 5 Hubbard Brook snow survey sites (with elevation) during the spring season, based on HBEF data from 1993 to 2015.

at 18.7 GHz were 239.1 K in the vertical polarization and 232.0 K horizontal. Differences between the 36.5 GHz vertical $T_{\rm B}$ on this date are larger than the calculated RMSE over the nine year period. Previous to this date a warming event occurred that may have resulted in a melt-refreeze layer in the snow causing increased scattering in the satellite data.

4.3.1. Homogenous distribution of LWC percentage

For the first sensitivity analysis, the same LWC was applied to each MEMLS grid cell as a percentage of the SWE in that cell, increasing by 0.1% increments from 0 to 5% LWC. With the initial application of 0.1% LWC, the average T_B across the domain increased by approximately 14.5 and 12.7 K for the vertical and horizontal polarizations, respectively (Fig. 6). The vertically polarized 36.5 GHz brightness temperatures continued to rise with increasing LWC until leveling off around 1% LWC. In contrast, the horizontally polarized 36.5 GHz channel decreased after the initial rise even with increasing amounts of liquid water in the snow. This is caused by further increases in the surface reflectivity (Kang et al., 2014). Both the horizontally and vertically polarized 18.7 GHz T_B changed to a smaller degree initially than the 36.5 GHz channel and then closely followed the corresponding polarization from the 36.5 GHz data as additional LWC was introduced to the snow pack. The remainder of this study focuses on the vertically polarized 36.5 GHz signal that has a strong response to liquid water and then remains constant.

4.3.2. Impact of snow properties

The LWC sensitivity analysis, using a homogenous LWC percentage across the domain, was repeated while adjusting the other snow characteristics to assess the impact on the 36.5 GHz vertical signal. The average snowpack depth over the domain was scaled from 25 to 80 cm by multiplying each pixel by the ratio of the new depth to the original depth. For dry conditions, the $T_{\rm B}$ values differ by 15.3 K with the lowest $T_{\rm B}$ estimated for the 80 cm snowpack (Fig. 7a). The initial application of 0.1% liquid water equalizes the $T_{\rm B}$ to the average snowpack temperature (266.8 K). Next, the domain average snow density was varied between 200 and 400 kg/m³ by similarly scaling the individual model cells. The initial $T_{\rm B}$ ranged between 237.4 and 258.4 K for the low- and high-density tests, respectively (Fig. 7b). Similar to snow depth, the $T_{\rm B}$ equalizes to the snowpack temperature with the addition of 0.1% LWC.

Adjusting the correlation lengths had a larger effect on the initial T_B with values for dry snow ranging from 91 to 250 K for $p_{\rm ex}$ values of 0.65 and 0.11 mm, respectively (Fig. 7c). These values were selected based on observed correlation lengths of fine and coarse snow grains (Mätzler and Wiesmann, 1999). With additional amounts of LWC, the T_B values converge on the snowpack temperature, though more LWC is required for T_B to reach the maximum temperature with larger snow grains. Finally, the grid cell snowpack temperatures were scaled to obtain domain-average temperature of 270 K, which is closer to what would realistically be expected during a melt event, when the snow temperature must be at the melting point. The snow temperature determines the maximum T_B value of the wet snowpack. In almost all cases, with the exception of the largest correlation length, the T_B reached a maximum T_B at approximately 1% LWC.

4.3.3. Effects of spatially distributed LWC to aggregated T_B signal

The next analysis considered the microwave response for a region in which part of the snowpack was wet and part was dry. A 1% LWC was assigned to a portion of the grid cells in the domain, increasing in area by 10% for each simulation, from 0 to 100%. $T_{\rm B}$ was modeled using MEMLS for each grid cell, then a single, average $T_{\rm B}$ values was calculated for the domain. The 1% LWC value was selected based on the results of the previous analysis when the maximum $T_{\rm B}$ value was typically reached despite variations in snow properties. Pixels were assigned LWC using two different spatial distributions. The first method assigned LWC randomly to grid cells. The second method assigned LWC by grid

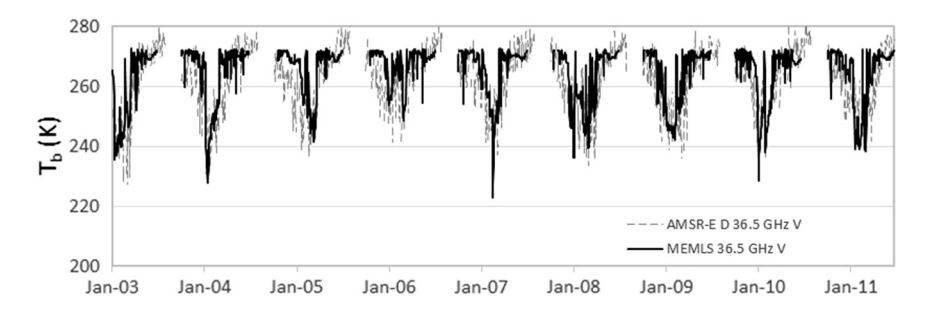


Fig. 4. Daily average T_B over study domain for water years 2003–2011, from model results and satellite retrievals.

cell elevation starting with the lowest elevations. Fig. 8 shows examples of the resulting T_B distribution when 1% LWC is assigned randomly (top row) and from low to high elevation (bottom row) over 20, 50 and 80% of the total area. In the randomly distributed examples, the spatial variation in T_B clearly decreases as a greater percentage of the area is wet, while the low T_B values at higher elevations persist when LWC is distributed by elevation. There is relationship between the portion of the area affected by wet snow and the change in T_B, with the maximum possible change in T_B occurring when 100% of the domain is affected (Fig. 9). When 1% LWC is randomly distributed over the domain the relationship follows a linear trend. When the LWC was distributed by elevation, the results nearly match the linear relationship of the randomly distribution though values are slightly depressed in the middle. The greatest difference in T_B when LWC is distributed randomly and by elevation is 1 K when 50% of the domain is affected. This reduced T_B when approximately half of the area is impacted is likely due to the deeper dry snow remaining at the higher elevations impacting the microwave emissions.

4.4. Wet snow events

4.4.1. Comparison of modeled wet snow events to sensitivity results

Over the 9-year period, 44 wet snow events were detected using a threshold change in $T_{\rm B}$ greater than 5 K from the previous day and limiting the analysis to the December to March time period when the

average SWE over the domain was at least 10 mm. Fig. 10 shows the wet snow events plotted along with the sensitivity analysis results when the LWC was distributed by elevation. There is good agreement between the modeled wet snow events and the sensitivity analysis results, indicating that despite variability in snow properties there is a relationship between areal extent of wet snow and the T_B response.

4.4.2. Comparison of modeled emission results to satellite retrievals

For each of the 44 wet snow events, the AMSR-E vertically polarized 36.5 GHz T_B was obtained for the study domain. In every case, during wet snow events identified in the modeled emission results, the AMSR-E T_B also increased. There is a positive relationship between the satellite observations and model T_B changes during each of the events; however there is also considerable scatter (Fig. 11) and the correlation is low, $R^2=0.13$. Despite the heavy mixed-forest tree canopy, the magnitude of the AMSR-E T_B changes is as large as the modeled changes. While, the presence of vegetation affects SWE estimation using passive microwave, the ability to detect wet snow events using the relative change in T_B signal still shows potential.

4.4.3. Evaluation of discharge response

Wet snow events indicate snowmelt and, in some cases, will be followed by streamflow increases. For the 370 km² Baker River watershed, the change in discharge, ΔQ , from the date of the T_B response to

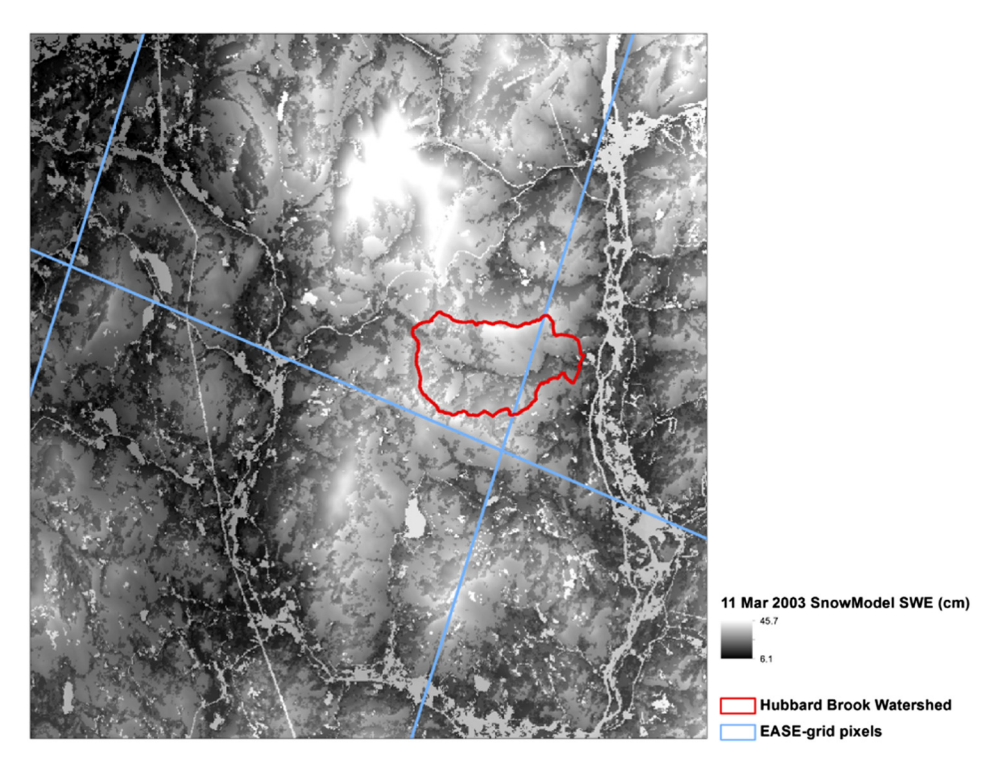


Fig. 5. SnowModel SWE on 11 Mar 2003 when domain was 100% snow covered with no LWC.

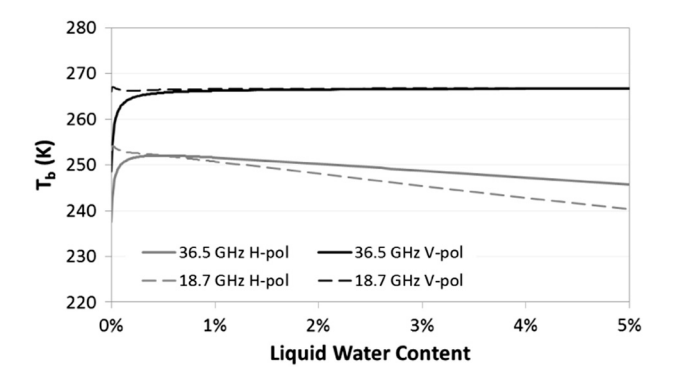


Fig. 6. Vertically and horizontally polarized 36.5 GHz $T_{\rm B}$ for increasing percent LWC, averaged over the study domain.

the peak flow, up to four days following the wet snow event, was evaluated. Fig. 12 shows the relationship between the increasing discharge and the increasing T_B from the model results and AMSR-E observations. In all cases, an increase in discharge followed the increase in T_B , though there is not a strong relationship between the magnitude of the T_B increase and discharge (correlation less than 0.1 for MEMLS and 0.22 for AMSR-E). In approximately 20% of the events the increase in discharge was small (less than 10% of the average peak annual flow, 29 cm), though the change in T_B was large. After reviewing temperature data in the region, many of these events represent early-season warming periods where the signal response is likely due to surface melt and which did not sufficiently warm the snowpack to cause runoff; therefore they did not result in significant increases in discharge. The comparison improves if we evaluate the events by month, though there is still a significant amount of scatter in the microwave response.

5. Discussion

The T_B response to the presence of liquid water in the snow dominates the emission signal. This signal has been identified in previous research as a potential indicator of melt onset. The results of this study agree with earlier research, which shows a sharp increase in the

measured 36.5 GHz T_B value with relatively low LWC values. Similarly, we found constant values for the vertically polarized T_B and decreases in horizontally polarized T_B with additional LWC above 1% (Kang et al., 2014). Snow depth, density and grain size have a strong impact on the measured T_B for dry snow, but the change in T_B with wet snow is clearly evident over a range of initial snow characteristics. In contrast to Kang et al. (2014), this study found that different grain sizes can yield a significant difference in the initial T_B response, though the resulting T_B once LWC is present is similar despite differences in snow properties.

Based on the sensitivity analysis performed in this study, there is a near linear relationship between the percent area where wet snow is present and the change in the aggregated T_B signal over that area. There is only a small difference in the relationship when the LWC is distributed randomly versus by elevation in this region. An accurate distribution is important to correctly estimate the discharge response; therefore additional information can be used to spatially distribute the disaggregated wet snow signal. During the ablation period, snowmelt is driven by energy fluxes that are influenced by topography, vegetation and solar radiation (Melloh et al., 2008). Several studies have observed repeated patterns in spatial distribution of melt using various techniques, such as digital imagery, terrestrial laser scans and remote sensing (Egli et al., 2012; Ide and Oguma, 2013), which could be used to describe the melt distribution.

The results of the sensitivity analysis were compared to actual wet snow events as detected by the combined snow-emission model results over a 9-year period. There is strong agreement between the percent area affected by wet snow and the change in T_B across a range of snow conditions and time periods. The comparison of modeled results to the AMSR-E T_B response during wet snow events yielded a moderate positive linear relationship. While all of the detected melt events saw a corresponding positive increase in AMSR-E T_B measured at 36.5 GHz, the correlation between the magnitudes of T_B changes was weak. This may be due to regional effects of vegetation on the satellite signal, or the area over which the area-weighted average was computed. Previous research has shown regional differences in the satellite sensor performance in estimating SWE as compared to modeled data (Vuyovich et al., 2014). Thus, the signal response should be investigated in different regions and domains.

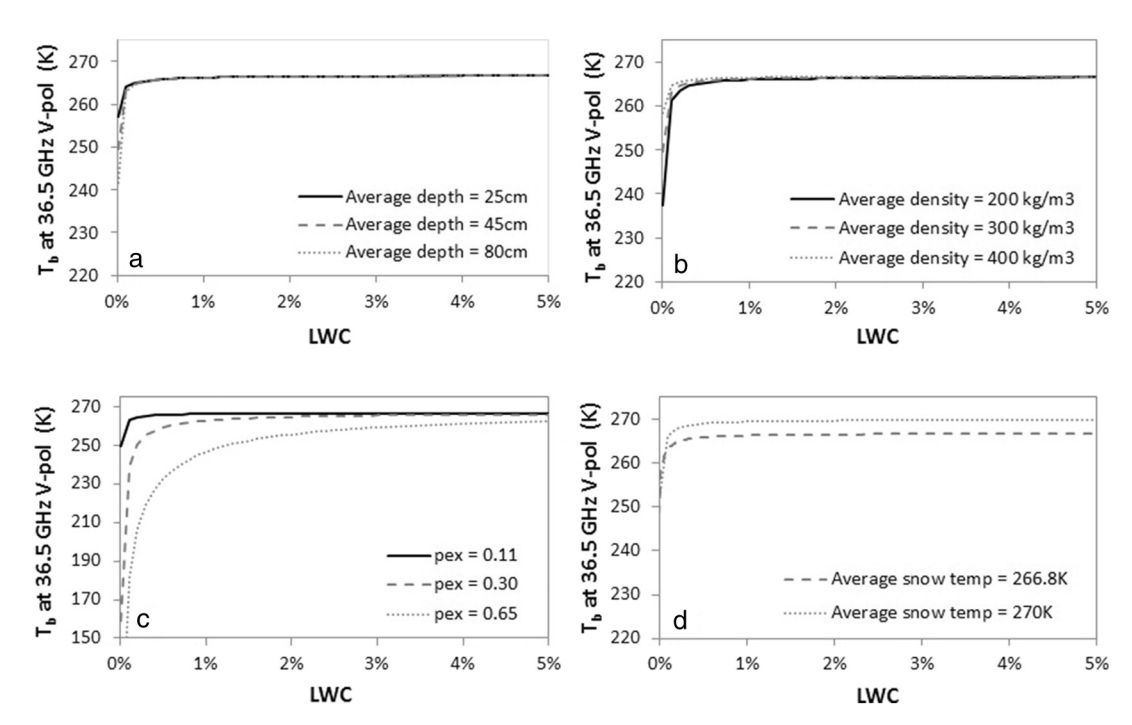


Fig. 7. Vertically polarized 36.5 GHz T_B for increasing percent LWC, averaged over the domain as a function of a. snow depth, b. snow density, c. correlation length, and d. snowpack temperature.

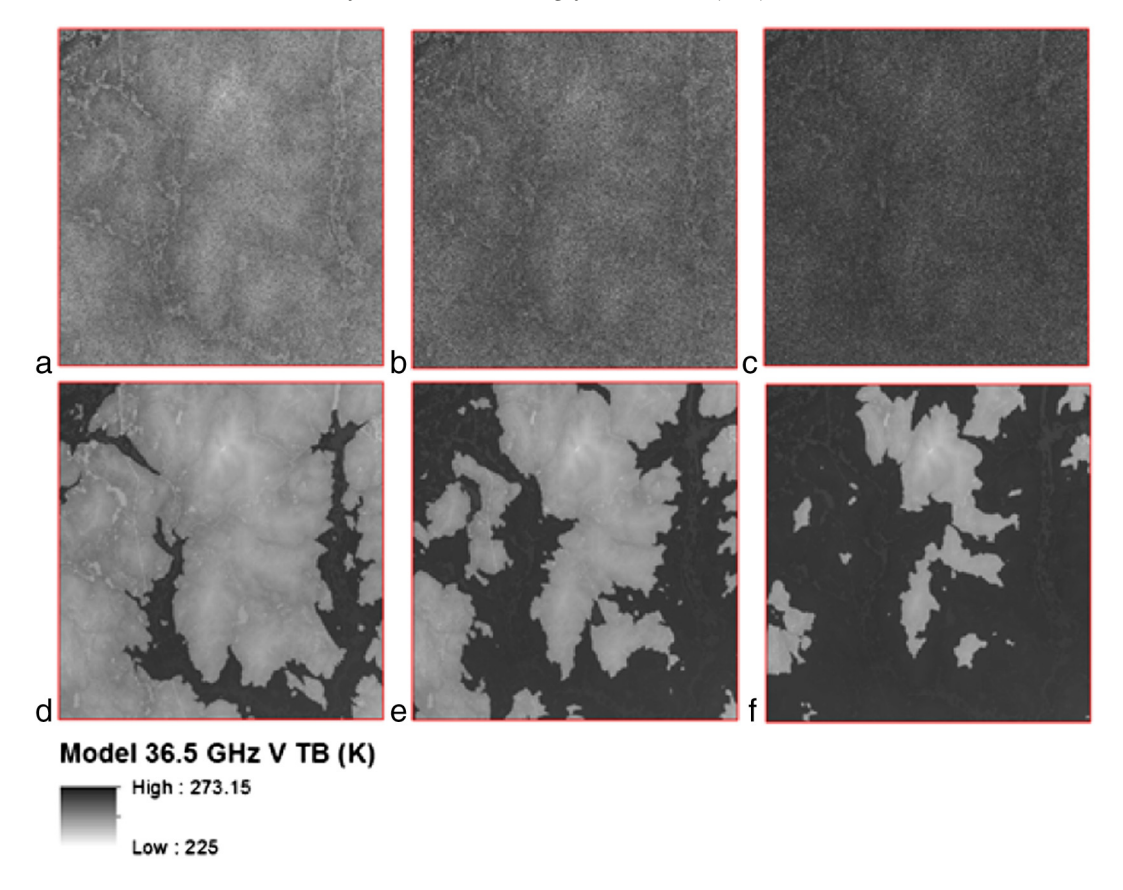


Fig. 8. T_{B, 36.5 V} resulting from 1% LWC distributed randomly (top row) and by elevation (bottom row) over 20% (a, d), 50% (b, e) and 80% (c, f) of the area.

The comparison of the wet snow signal response and the discharge at a station within the domain showed a positive relationship between increased T_B and increased discharge. It is encouraging to see a response at such a small scale, particularly given the temporal resolution of the model. Yan et al. (2009) used the melt signal from DAV and a conceptually-based hydrologic model to predict spring snowmelt over a large Alaskan basin. While their hydrograph timing results were accurate in most years, they acknowledge limitations of running at such a coarse resolution (to match EASE-grid pixel size), and the need for better snowpack characterization. This study provides the potential basis for disaggregating melting snow within the microwave pixel based on the T_B response.

6. Conclusion

Satellite-based, passive microwave data have been investigated over multiple decades for their ability to provide global snow information. Over much of that time the signal response to liquid water in the snow-pack has been examined for its potential to predict snowmelt onset timing. This study expanded earlier work by Kang et al. (2014) and Pan et al. (2014), investigating the sensitivity of microwave emission at a point, by evaluating the emission response to spatially distributed LWC. A sensitivity analysis was conducted using synthetic distributions of LWC over a realistically distributed snowpack. An increasing, nearlinear relationship was found between the T_B signal response and the

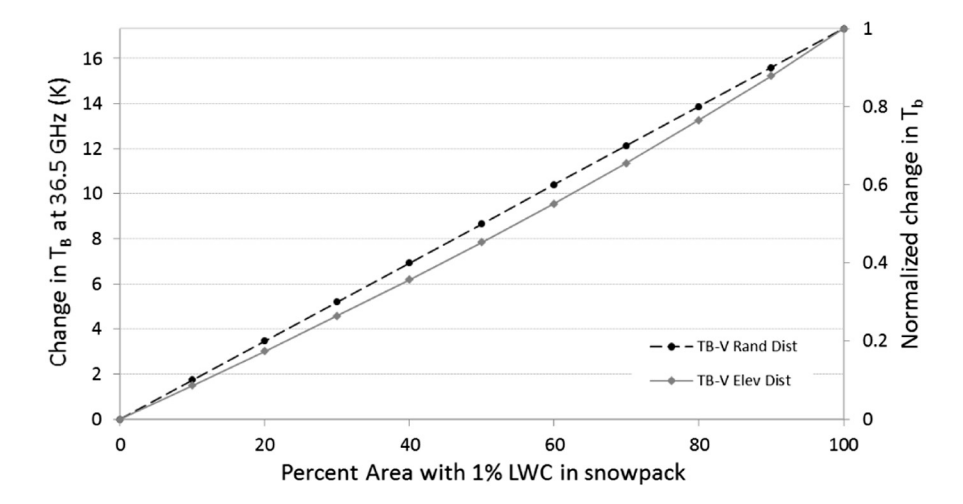


Fig. 9. Change in average T_B over the domain as a function of percent area with 1% LWC assigned to pixels in MEMLS sensitivity analysis; assignment was randomly distributed (black dash line) and distributed by elevation (gray line).

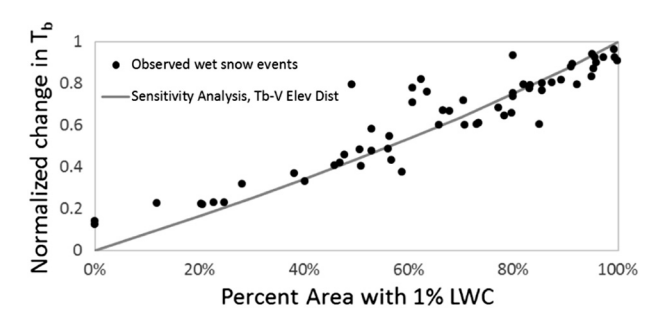


Fig. 10. Normalized change in T_B (Eq. (1)) for wet snow events and results of the sensitivity analysis when LWC was distributed by elevation.

percent area with LWC present, suggesting that the microwave response provides the potential basis for disaggregating melting snow within a microwave pixel. The results were confirmed by evaluating actual wet snow events over a 9-year period. These results have important implications on the potential use of microwave data to inform not only the melt timing but also the magnitude of runoff. Operational snow hydrology models require estimates of initial snowpack characteristics to accurately estimate melt timing and magnitude. Future work should evaluate the utility of microwave data to initialize model snow state based on the wet snow response.

Wet snow events identified in the microwave signal were compared to discharge data for a basin within the domain. An increase in T_B was followed by a subsequent increase in discharge in all cases; however the magnitude of the change did not correspond. Next steps should include evaluating the spatial distribution of wet snow in larger basins to understand the hydrological impact of large-scale snowmelt events as detected by passive microwave data. The microwave signal should be evaluated across different regions where the satellite-based wet snow signal may provide useful information. Future work should also investigate whether the relationship holds in other snow regimes, such as a homogenous plains snowpack or deep mountain snowpack with high spatial variability.

Acknowledgements

This work was supported by a NASA ESPCOR Grant: NNX11AQ34A, Passive Microwave Detection of Snowmelt and Runoff; a NASA ROSES Grant: NNH13ZDA001N, Satellite Enhanced Snowmelt Flood Predictions in the Red River of the North Basin; a NASA Terrestrial Hydrology Grant: NNH14AX42I, Blending Fine-Scale Terrestrial Snow Information with Coarse-Scale Remote Sensing Data Using Inferential and Modeling

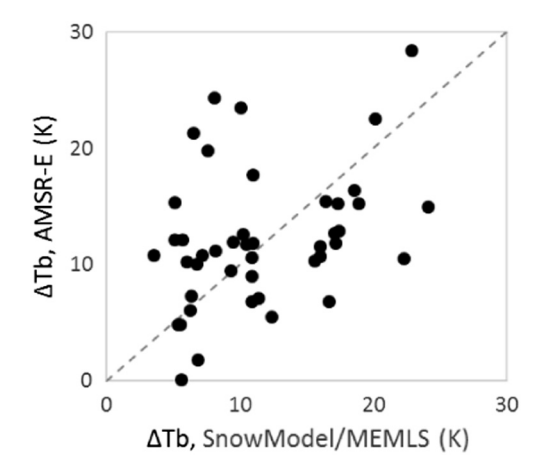


Fig. 11. Change in T_B corresponding to wet snow events from MEMLS and AMSR-E, with 1:1 line

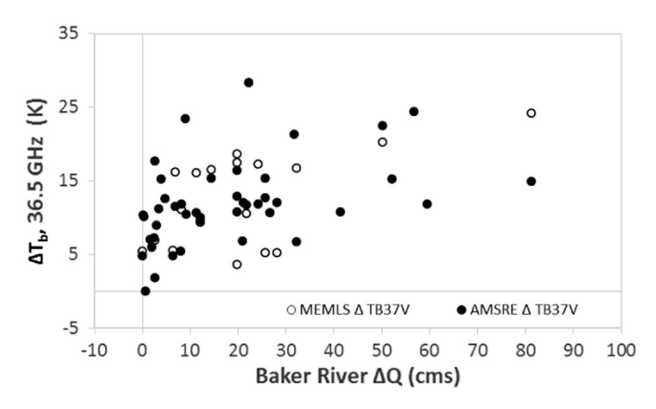


Fig. 12. Modeled and observed temperature brightness changes versus discharge increase at the Baker River gage following wet snow events.

Methods; and the U.S. Army Terrestrial Environmental Modeling & Intelligence System (ARTEMIS) applied science research program sponsored by the Assistant Secretary of the Army for Acquisition, Logistics, and Technology (ASA-ALT). We would also like to thanks the three anonymous reviewers whose suggestions greatly improved the paper.

References

Bailey, A.S., Hornbeck, J.W., Campbell, J.L., Eagar, C., 2003. Hydrometeorological database for Hubbard Brook Experimental Forest: 1955–2000. Gen. Tech. Rep. NE-305. USDA Forest Service Northeastern Research Station, Newtown Square, PA, p. 36.

Bales, R.C., Molotch, N.P., Painter, T.H., Dettinger, M.D., Rice, R., Dozier, J., 2006. Mountain hydrology of the western United States. Water Resour. Res. 42, 13.

Cagnati, A., Crepaz, A., Macelloni, G., Pampaloni, P., Ranzi, R., Tedesco, M., Tomirotti, M., Valt, M., 2004. Study of the snow melt-freeze cycle using multi-sensor data and snow modelling, J. Glaciol. 50, 419–426.

Campbell, J.L., Driscoll, C.T., Eagar, C., Likens, G.E., Siccama, T.G., Johnson, C.E., Fahey, T.J., Hamburg, S.P., Holmes, R.T., Bailey, A.S., Buso, D.C., 2007. In: U.S.D.o. Agriculture (Ed.), Long-term Trends From Ecosystem Research at the Hubbard Brook Experimental Forest. USDA Forest Service, Newton Square, PA.

Campbell, J.L., Driscoll, C.T., Pourmokhtarian, A., Hayhoe, K., 2011. Streamflow responses to past and projected future changes in climate at the Hubbard Brook Experimental Forest, New Hampshire, United States. Water Resour. Res. 47, 15.

Cavalieri, D.J., Markus, T., Comiso, J.C., 2014. In: NASA (Ed.), AMSR-E/Aqua Daily L3 25 km
Brightness Temperature & Sea Ice Concentration Polar Grids, Version 3. National
Snow and Ice Data Center Distributed Active Archive Center. Boulder. CO USA.

Chang, A.T.C., Foster, J.L., Hall, D.K., Rango, A., Hartline, B.K., 1982. Snow water equivalent estimation by microwave radiometry. Cold Reg. Sci. Technol. 5, 259–267.

Clifford, D., 2010. Global estimates of snow water equivalent from passive microwave: history, challenges and future developments. Int. J. Remote Sens. 31 (14): 3707–3726. http://dx.doi.org/10.1080/01431161.2010.483482.

Davis, R.E., Dozier, J., Chang, A.T.C., 1987. Snow property measurements correlative to microwave emission at 35 GHz. IEEE Trans. Geosci. Remote Sens. 25, 751–757.

Derksen, C., Walker, A., Goodison, B., 2003. A comparison of 18 winter seasons of in situ and passive microwave-derived snow water equivalent estimates in Western Canada. Remote Sens. Environ. 88:271–282. http://dx.doi.org/10.1016/j.rse.2005.02.014.

Dozier, J., Bair, E.H., Davis, R.E., 2016. Estimating the spatial distribution of snow water equivalent in the world's mountains. Wiley Interdiscip. Rev. Water 3, 461–474.

Drobot, S.D., Anderson, M.R., 2001. An improved method for determining snowmelt onset dates over Arctic sea ice using scanning multichannel microwave radiometer and special sensor microwave/imager data. J. Geophys. Res.-Atmos. 106, 24033–24049.

Egli, L., Jonas, T., Grunewald, T., Schirmer, M., Burlando, P., 2012. Dynamics of snow ablation in a small Alpine catchment observed by repeated terrestrial laser scans. Hydrol. Process. 26, 1574–1585.

Elder, K., Rosenthal, W., Davis, R.E., 1998. Estimating the spatial distribution of snow water equivalence in a montane watershed. Hydrol. Process. 12, 1793–1808.

Foster, J., Sun, C., Walker, J., Kelly, R., Chang, A., Dong, J., Powell, H., 2005. Quantifying the uncertainty in passive microwave snow water equivalent observations. Remote Sens. Environ. 94:187–203. http://dx.doi.org/10.1016/j.rse.2004.09.012.

Gandin, L.S., 1965. Objective Analysis of Meteorological Fields. Israel Program for Scientific Translations (242 pp.).

Green, R.O., Dozier, J., Roberts, D., Painter, T., 2002. Spectral snow-reflectance models for grain-size and liquid-water fraction in melting snow for the solar-reflected spectrum. Ann. Glaciol. 34, 71–73.

Grenfell, T.C., Putkonen, J., 2008. A method for the detection of the severe rain-on-snow event on Banks Island, October 2003, using passive microwave remote sensing. Water Resour. Res. 44:3. http://dx.doi.org/10.1029/2007WR005929.

Homer, C., Dewitz, J., Yang, L.M., Jin, S., Danielson, P., Xian, G., Coulston, J., Herold, N., Wickham, J., Megown, K., 2015. Completion of the 2011 national land cover database for the conterminous United States - representing a decade of land cover change information. Photogramm. Eng. Remote. Sens. 81, 345–354.

- Ide, R., Oguma, H., 2013. A cost-effective monitoring method using digital time-lapse cameras for detecting temporal and spatial variations of snowmelt and vegetation phenology in alpine ecosystems. Eco. Inform. 16, 25–34.
- Kang, D.H., Barros, A.P., Dery, S.J., 2014. Evaluating passive microwave radiometry for the dynamical transition from dry to wet snowpacks. IEEE Trans. Geosci. Remote Sens. 52, 3–15.
- Kopczynski, S.E., Ramage, J., Lawson, D., Goetz, S., Evenson, E., Denner, J., Larson, G., 2008. Passive microwave (SSM/I) satellite predictions of valley glacier hydrology, Matanus-ka Glacier. Alaska. Geophys. Res. Lett. 35.
- Kunzi, K., Patil, S., Rott, H., 1982. Snow-cover parameters retrieved from Nimbus-7 scanning multichannel microwave radiometer (SMMR) data. IEEE Trans. Geosci. Remote Sens. GE-20 (4), 452–467.
- Liston, G.E., Elder, K., 2006a. A distributed snow-evolution modeling system (SnowModel). I. Hydrometeorol. 7. 1259–1276.
- Liston, G.E., Elder, K., 2006b. A meteorological distribution system for high-resolution terrestrial modeling (MicroMet). J. Hydrometeorol. 7, 217–234.
- Liston, G.E., Hiemstra, C.A., 2008. A simple data assimilation system for complex snow distributions (SnowAssim). J. Hydrometeorol. 9, 989–1004.
- Lundquist, J.D., Dettinger, M.D., 2005. How snowpack heterogeneity affects diurnal streamflow timing. Water Resour. Res. 41, 14.
- Lundquist, J.D., Cayan, D.R., Dettinger, M.D., 2004. Spring onset in the Sierra Nevada: when is snowmelt independent of elevation? J. Hydrometeorol. 5, 327–342.
- Mätzler, C., 1987. Applications of the interaction of microwaves with the natural snow cover. Remote Sens. Rev. 2, 259–387.
- Mätzler, C., Wiesmann, A., 1999. Extension of the microwave emission model of layered snowpacks to coarse-grained snow. Remote Sens. Environ. 70, 317–325.
- Mätzler, C., Schanda, E., Hofer, R., Good, W., 1980. Microwave signatures of the natural snow cover at Weissfluhjoch. Proceedings of the NASA Workshop on Microwave Rem. Sens, of Snowpack Properties. NASA Conf. Publ. 2153, pp. 203–223.
- Melloh, R.A., Richmond, P., Shoop, S.A., Affleck, R.T., Coutermarsh, B.A., 2008. Continuous mapping of distributed snow depth for mobility models using shaped solutions. Cold Reg. Sci. Technol. 52, 155–165.
- Nagler, T., Rott, H., 2000. Retrieval of wet snow by means of multitemporal SAR data. IEEE Trans. Geosci. Remote Sens. 38 (2), 754–765.
- Nghiem, S.V., Tsai, W.-Y., 2001. Global snow cover monitoring with spaceborne Ku-band scatterometer. IEEE Trans. Geosci. Remote Sens. 39 (10), 2118–2134.
- Pan, J.M., Jiang, L.M., Zhang, L.X., 2014. Comparison of the multi-layer HUT snow emission model with observations of wet snowpacks. Hydrol. Process. 28, 1071–1083.
- Proksch, M., Lowe, H., Schneebeli, M., 2015. Density, specific surface area, and correlation length of snow measured by high-resolution penetrometry. J. Geophys. Res. Earth Surf. 120, 346–362.
- Ramage, J., Semmens, K.A., 2012. Reconstructing snowmelt runoff in the Yukon River basin using the SWEHydro model and AMSR-E observations. Hydrol. Process. 26, 2563–2572.

- Ramage, J.M., McKenney, R.A., Thorson, B., Maltais, P., Kopczynski, S.E., 2006. Relationship between passive microwave-derived snowmelt and surface-measured discharge, Wheaton River, Yukon Territory, Canada. Hydrol. Process. 20, 689–704.
- Rawlins, M.A., McDonald, K.C., Frolking, S., Lammers, R.B., Fahnestock, M., Kimball, J.S., Vorosmarty, C.J., 2005. Remote sensing of snow thaw at the pan-Arctic scale using the SeaWinds scatterometer. I. Hydrol. 312. 294–311.
- Semmens, K.A., Ramage, J., Bartsch, A., Liston, G.E., 2013. Early snowmelt events: detection, distribution, and significance in a major sub-arctic watershed. Environ. Res. Lett. 8, 11
- Stiles, W.H., Ulaby, F.T., 1980. The active and passive microwave response to snow parameters. 1. Wetness. J. Geophys. Res. Oceans Atmos. 85, 1037–1044.
- Tedesco, M., 2015. Remote Sensing of the Cryosphere. The Cryosphere Science SeriesWiley-Blackwell.
- Tedesco, M., Kim, E.J., 2006. Intercomparison of electromagnetic models for passive microwave remote sensing of snow. IEEE Trans. Geosci. Remote Sens. 44, 2654–2666.
- Tedesco, M., Kim, E.J., England, A.W., De Roo, R.D., Hardy, J.P., 2006. Brightness temperatures of snow melting/refreezing cycles: Observations and modeling using a multi-layer dense medium theory-based model. IEEE Trans. Geosci. Remote Sens. 44, 3563-3573
- Tedesco, M., Brodzik, M., Armstrong, R., Savoie, M., Ramage, J., 2009. Pan arctic terrestrial snowmelt trends (1979–2008) from spaceborne passive microwave data and correlation with the Arctic Oscillation. Geophys. Res. Lett. 36, 6.
- USGS, 2001. National Water Information System data available on the World Wide Web (Water Data for the Nation). U.S.G. Survey.
- USGS, 2009. National Elevation Dataset (NED). U.S.G.S. (USGS) (Sioux Falls, SD).
- Vuyovich, C., Jacobs, J.M., 2011. Snowpack and runoff generation using AMSR-E passive microwave observations in the Upper Helmand Watershed, Afghanistan. Remote Sens. Environ. 115, 3313–3321.
- Vuyovich, C.M., Jacobs, J.M., Daly, S.F., 2014. Comparison of passive microwave and modeled estimates of total watershed SWE in the continental United States. Water Resour. Res. 50, 9088–9102.
- Walker, A.E., Goodison, B.E., 1993. Discrimination of a wet snow cover using passive microwave satellite data. Ann. Glaciol. 17, 307–311.
- Wang, H., Arslan, A.N., Pulliainen, J., Hallikainen, M., 2001. Microwave emission model for wet snow by using radiative transfer and strong fluctuation theory. J. Electromagn. Waves Appl. 15, 57–59.
- Wiesmann, A., Mätzler, C., 1999. Microwave emission model of layered snowpacks. Remote Sens. Environ. 70, 307–316.
- Wiesmann, A., Mätzler, C., Weise, T., 1998. Radiometric and structural measurements of snow samples. Radio Sci. 33, 273–289.
- Yan, F.L., Ramage, J., McKenney, R., 2009. Modeling of high-latitude spring freshet from AMSR-E passive microwave observations. Water Resour. Res. 45, 14.